applied sciences

MDPI

Review

Heavy Metal Ion Detection Platforms Based on a Glutathione Probe: A Mini Review

Jian Zhang [1,2], Xuan Sun [1] and Jayne Wu [2,*]

[1] School of Electronic Science and Applied Physics, Hefei University of Technology, Hefei 230009, China; zhangjian@hfut.edu.cn (J.Z.); 15056283230@163.com (X.S.)

[2] Department of Electrical Engineering and Computer Science, The University of Tennessee, Knoxville, TN 37996, USA

* Correspondence: jaynewu@utk.edu

Received: 14 December 2018; Accepted: 23 January 2019; Published: 31 January 2019

Featured Application: Rapid, sensitive and low cost detection of heavy metal ions can be readily achieved by various sensing strategies using glutathione as a molecular probe.

Abstract: Globally, heavy metal ion (HMI) contamination is on the rise, posing an ever-increasing risk to ecological and human health. In recent years, great research effort has been devoted to the sensitive detection and quantitative analysis of HMIs. Low cost, sensitive, selective, and rapid methods for HMI detection are of growing demand, and HMI biosensors have great potential in meeting this need due to their timeliness, cost-effectiveness and convenience in operation. Glutathione is known for its strong ability to bind with toxic heavy metal ions, in addition to its water solubility, stable activity and ready availability. As a result, glutathione is becoming a molecular probe of choice in the preparation of sensors for sensitive, affordable, and accessible HMI detection. This review summarizes the results from various glutathione-based HMI detection strategies reported in recent years, which are categorized according to their signal transduction methods. Their operation and implementation, along with figures of merit such as limit of detection, selectivity, and response time, are discussed and compared. Based on the review, both individual HMI detection and simultaneous detection of multiple HMIs can be realized under specific reaction conditions, showing the great potential of glutathione-based detection to realize various types of practical HMI detection.

Keywords: heavy metal ions; glutathione; biosensor; nanoparticle

1. Introduction

In general, heavy metals are the metals with relatively high mass densities (above 5 g/cm^3), such as platinum, gold, mercury, and lead. The definition of heavy metals varies from discipline to discipline due to different concerns and perspectives. For physiology and pathology, heavy metals mainly refer to heavy elements with obvious biotoxicity. In terms of toxicity, the most common heavy metals include lead (Pb), mercury (Hg), arsenic (As), cadmium (Cd), and chromium (Cr) [1–4]. These heavy metal ions (HMIs) accumulate in the human body and cause chronic poisoning, resulting in damage to the immune, gastrointestinal, reproductive, and nervous systems [5–7]. Long-term exposure to heavy metals may even cause cancer in humans [8]. Being non-biodegradable, HMIs will continue to exist for decades and even hundreds of years if they are released into the environment [9]. With increasing human activities in mining and manufacturing, etc., HMI contamination and pollution pose great risks to ecological and human health [10,11]. Therefore, it is of great importance to be able to effectively screen for and quantitatively determine HMIs in a range of situations, including food safety, environmental pollution, and clinical diagnosis. Many international organizations and regulatory

bodies, such as the World Health Organization (WHO) and the U.S. Environmental Protection Agency (EPA), have listed heavy metals as priority substances for intensive monitoring [1]. In practice, most countries have set standards on the permissible limits for HMI concentrations in water or other mediums to protect the environment and public health.

Traditional HMI measurements are mostly performed using spectroscopic techniques, including atomic absorption spectroscopy (AAS) [4,12], X-ray fluorescence spectrometry (XRF) [4,13], and inductively coupled plasma mass spectrometry (ICP-MS) [4,14], which are gold standards in HMI detection. However, they are expensive, difficult to perform, require complicated pretreatment for the samples, and need to be operated in a central laboratory setting. Thus, traditional spectroscopic techniques cannot meet the needs for pervasive HMI monitoring and screening. In contrast, surface-based biosensors are a good candidate to realize low-cost, sensitive HMI detection with a quick turn-around time. Similar to other biochemical sensors, there are three important components in an HMI sensor: analyte recognition, physical support for probe immobilization, and signal transduction. Various types of sensors have been reported, including nanoparticles [15–17], field effect transistors (FETs) [18–20], and working electrodes for voltammetric analysis [21]. In terms of signal transduction, there are mainly optical [15] and electrochemical methods [4]. Specific target recognition is always critically important to analyte detection. Antibody [22], nuclei acids [23,24], and peptide/amino acids [25,26] are the most commonly used probes to recognize and bind with HMIs. An antibody as a probe has the best specificity, but faces challenges when detecting HMIs. HMIs are too small to be directly detected with good sensitivity by an antibody, and antibody binding reactions may require a fluid environment different from that HMIs naturally exist in. Two types of functional nuclei acid probes have been developed for metal sensing: aptamers and DNAzymes. It is well-known that screening aptamer sequences to find one that specifically binds with a certain HMI is difficult, in addition to being laborious and time-consuming. Very few metal ions have successfully found their specific aptamers [27,28]. DNAzymes can selectively detect HMIs based on their catalytic activity; however, another nuclei acid sequence is required to be added to work as the substrate–enzyme pair. During metal detection by DNAzyme, additional steps and time are needed to allow for catalytic reactions between the DNAzyme and the substrate. Besides antibodies, aptamers, and DNAzyme, another option is to use a peptide or an amino acid as a probe to bind with HMIs, such as cysteine [29]. The most widely reported peptide probe for HMI detection is glutathione (GSH) [30]. Because there are six possible coordination sites in GSH for binding with metal ions, it has distinct advantages in capturing HMIs when compared with cysteine, especially in case of lead ion (Pb^{2+}) detection. Furthermore, it is highly stable, cost-effective, and easy to immobilize on a sensor. Therefore, GSH, as a promising probe for HMI detection, has received much attention in recent years.

In this review, the chemical properties of GSH and its coordination with HMIs are briefly discussed first. Then, various GSH-based HMI detection strategies are reviewed and discussed. GSH-based HMI detection is categorized according to the signal transduction mechanisms, mainly optical methods and electrochemical methods. For optical detection methods, two formats have been reported, which are metal-nanoparticle-based platforms and semiconductor quantum-dot-based platforms. For electrochemical methods, the sensor structures can be mainly categorized into field effect transistors and working electrodes. Then, the performance of different HMI detection platforms is summarized, and future challenges are discussed.

2. Recognition of HMIs by GSH

Glutathione (GSH) is a ubiquitous tripeptide biomolecule (γ-Glu-Cys-Gly) widely found in animals and plants with a concentration from 0.1 mM to 10 mM [31]. GSH is known as an antidote to prevent cells from toxicosis of heavy metal ions by forming complexes as a key step in biological detoxification processes [30].

The chemical structure of GSH is shown in Figure 1. If oxidized, GSH will form disulfide bonds between themselves, and become what is known as glutathione disulphide (GSSG). GSSG lacks the

ability to bind with electrodes or nanoparticles. In practice, GSH in its reduced form is used to bind with HMIs. Reduced GSH is a linear tripeptide of L-glutamine, L-cysteine, and glycine, so reduced GSH is also labeled as L-GSH. GSH contains one amino (-NH2), one sulfhydryl (-SH), and two carboxyl (-COOH) groups, all with the ability to bind with HMIs. Therefore, GSH is a versatile ligand with several binding modes.

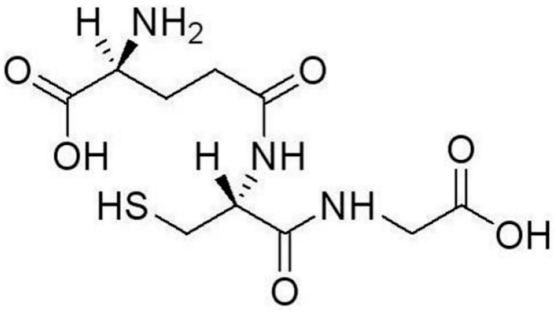

Figure 1. Glutathione's Chemical Structure.

GSH has a sulfhydryl group on the cysteinyl portion. The sulfhydryl group is known to coordinate with a wide range of metal ions. For surface-based or nanoparticle-based HMI sensors, GSH is usually immobilized on gold nanoparticles or electrodes. Numerous experiments indicate that there is a strong binding force between gold and the (-SH) group. It is expected that, during probe immobilization, Au–S bonds are formed to link GSH molecules onto the gold surface [32–35]. As a result, only one amino ($-NH_2$) and two carboxyls (-COOH) are still available to bind with metal ions.

A number of published papers have demonstrated that via the two free (-COOH) groups, strong binding with Pb^{2+} is preferred over that with other HMIs [35–37]. It was found that the solution pH has a strong effect on the affinity of the GSH–Pb^{2+} complex. At around pH 7, (-COOH) is deprotonated to (-COO-). Known as an oxyphilic ion, Pb^{2+} can combine with four acetate molecules or eight oxygen atoms [33]. Within a pH range of 4–8, binding between Pb^{2+} and (-COO-) will predominate over other reactions. Under the same pH condition, ($-NH_2$) is protonated to ($-NH_3^+$), which is hypothesized to prevent GSH from combining with other ions due to its charges [33,37]. Therefore, good affinity and selectivity can be achieved for GSH–Pb^{2+} binding. There exist a number of reports on using GSH to specifically detect Pb^{2+} from a mixture of multiple HMIs.

Nevertheless, detection of metal ions other than Pb^{2+} can also be achieved using GSH-based sensors. The GSH support material and the solution pH value play an important role in the HMI–GSH complexation pattern. Research has shown that GSH's conformational structure is strongly influenced by the solution pH [38]. Various functional groups in GSH can participate in complexation under different working conditions, leading to a certain selectivity. For example, GSH-capped quantum dots (QDs) are often used to detect HMIs other than Pb^{2+}. In [39], GSH immobilized on sulfur- and nitrogen-co-doped carbon QDs presented free (-SH) groups for binding, which showed strong affinity to Hg^{2+} as opposed to other metal ions (Ag^+, Al^{3+}, Ba^{2+}, Cu^{2+}, Pb^{2+}, etc.) and realized specific detection of Hg^{2+}. Simultaneous detection of Cr^{2+} and Pb^{2+} was reported using GSH-coated magnetic nanoparticles (NPs) [40], as GSH molecules were immobilized onto Fe_3O_4 NPs through a hydrogen bond. In this detection scheme, NH^{4+}, Na^+, Mg^{2+}, Hg^{2+} and other MIs caused no obvious responses, except for Cd^{2+} and Pb^{2+}. This was attributed in part to the negative charges on the functional groups of GSH [40], since the testing was done at a pH of 4.5. Simultaneous detection of multiple HMIs is thus possible by adjusting the solution pH and the GSH immobilization strategy. However, complexation reactions between GSH and HMIs are complicated and difficult to predict, and the detection outcome under particular conditions usually needs to be verified through experimental results.

The foregoing introduces the interactions and formation of complexes between GSH and HMIs, which are the basis for the specific recognition of certain HMIs by GSH-based detection methods. To convert specific binding between GSH and HMIs into a quantifiable signal, a transducer is needed,

which can take many different shapes and forms. Transduction schemes may have effects on the sensor performance as well, especially the plasmon-based detection that depends on the interaction between metal ions and nanoparticles. In next section, various GSH-based detection platforms are presented and discussed, with a focus on optical and electrochemical methods.

3. Heavy Metal Ion Detection Platforms Using Glutathione

Based on a signal transduction strategy, most of the GSH-based HMI detection methods can be categorized into two groups: optical methods and electrochemical methods. Then, each method is further divided into subtypes based on the support materials for GSH.

3.1. Optical Techniques

3.1.1. Metallic-Nanoparticle-Based Platforms

Metallic nanoparticles (NPs) are between 1–100 nm in size with a high surface charge density, a high surface to volume ratio, and, oftentimes, special optical properties due to a localized surface plasmon resonance (LSPR) effect. For these reasons, metallic NPs have been widely used in diverse biological and chemical applications, especially for biochemical detection. Various types of biochemical molecules can be easily incorporated onto the NPs while retaining their biochemical activity. For HMI detection, most metallic NPs are made of gold and some are silver, with gold NPs (GNPs) being the most widely used material in HMI sensors. Other shapes of NPs, such as nanorods and nanostars, have been adopted for sensing [41,42].

From the instrumentation point of view, two types of optical methods are commonly reported for Pb^{2+} detection: colorimetric and fluorescent detection. Other types of optical transduction techniques, such as an LSPR sensor (detection of molecular interactions near a nanostructured metal surface through shifts in the LSPR spectral peak) and dynamic light scattering (DLS) have also been reported. Fundamentally, the NP-based colorimetric assay is also based on the phenomenon known as LSPR. In assays based on noble metal NPs, as is well-known, there are a large number of free electrons on the metal surface. When incident photons resonate with free electrons on the NP surface, it will cause a collective charge oscillation. This in turn generates surface plasmon waves, leading to strong electromagnetic fields on the NP surface and enhanced light adsorption and scattering. The plasmon resonance frequencies of gold and silver NPs are generally in the 600–750 nm and 400–550 nm spectral ranges, respectively. Both LSPR sensors and colorimetric assays have been adopted in heavy metal ion detection. Molecular interactions between metal ions and the ligands on NPs will result in changes in the local refractive index near the NP surface. The changes in the refractive index of the surrounding environment is approximately linear with the LSPR peak wavelength shift. In practice, an LSPR sensor is mostly a surface-based method, while a colorimetric assay is solution-based. Typically, LSPR sensors are implemented using a surface with metallic nanostructures, which is functionalized with ligands to bind with metal ions. Binding between the ligands and the metal ions leads to the formation of a self-assembled monolayer (SAM) on the sensor surface. To find changes in the refractive index of a sensor's SAM, a spectral analysis is applied on the SAM film to find the shift in the LSPR peak wavelength. Due to the small size of the metal ions that are added to the SAM during testing, an extinction measurement is usually used. Colorimetric detection is based on the size-dependent optical property and aggregation/dispersion of metal NPs in a solution. Because particle aggregates are of a large size, about tens of nm, in large quantities, a spectral absorbance measurement is often used, and sometimes the color change can be observed by the naked eye.

An LSPR sensor for Pb^{2+} detection was developed using GSH-functionalized GNPs in [33]. In this report, GNPs were immobilized on a transparent indium tin oxide (ITO) glass substrate, then the ITO/GNPs stripes were functionalized with GSH. The ITO/AuNPs/GSH was used as a plasmonic probe. When the binding between GSH and Pb^{2+} occurred, the local refractive index at the ITO/AuNPs/GSH surface changed. As a result, a red-shift in the LSPR peak wavelength was observed when Pb^{2+} was

added into the solution. The Pb^{2+} detection was performed at pH 7.5, which was demonstrated to be a suitable pH value to recognize Pb^{2+}. This platform achieved a limit of detection (LOD) of 50 pM in 15 min, with a good selectivity against other MIs, such as Hg^{2+}, Cu^{2+}, Mg^{2+}, and Na^{+}.

Colorimetry is based on measuring the change in peak absorption wavelength between the dispersed and aggregation modes of NPs, which is caused by the addition of target analytes into a testing solution. Any change in the size, shape, or geometry of NPs will change the local electron confinement, leading to a change in the absorption maxima. Then, the color of the colloidal solution will change. This change between dispersion and aggregation and the subsequent color change is the basis of colorimetric detection when using metallic NPs to detect specific metal ions. A colorimetric method was developed for Pb^{2+} detection using GSH-functionalized GNPs (GSH-GNPs) in [43]. Normally, GSH can inhibit the aggregation of GNPs in solutions with a high concentration of salt. A carboxylate anion of GSH capping the GNPs will exhibit strong interparticle electrostatic repulsion between GNPs. When Pb^{2+} are added, complexes will form between Pb^{2+} and the carboxyl group of GSH. As a result, the stability of GSH-GNPs are reduced, making GNPs aggregate even under the high salt concentration in solution. Because the color of the GNP solution depends on the GNP size or aggregates, Pb^{2+} detection can then be achieved by a colorimetric analysis, either using a UV-vis spectrophotometer or naked eyes.

In [43], Pb^{2+} was detected by the colorimetric response of GSH-capped GNPs, with the color turning from red to purple in the presence of Pb^{2+}. During testing, NaCl-based aqueous solution was added to the samples to reach a high salt content. The limit of detection (LOD) was found to be 100 nM. After the addition of Zn^{2+}, Co^{2+}, Fe^{2+}, and eight other types of metal ions, all at 50 μM, negligible responses were observed in contrast to that of 20 μM Pb^{2+}, indicating that this approach is a specific platform to detect Pb^{2+}. Based on the transient curve of the absorption ratio (A700/520), the response time was optimized to be 25 min.

For fluorescence-based detection, a turn-on fluorescent nanoprobe for Pb^{2+} with a fast response was reported recently [44]. The working mechanism is aggregation-induced emission (AIE), which is considered to be an effect induced by a ligand-to-metal-metal charge transfer (LMMCT) through Au–S motifs due to aurophilic interactions. In [44], GSH was used as a thiolate ligand to detect Pb^{2+}. GNPs capped with GSH via an Au–S bond were synthesized first. When Pb^{2+} was added into the system, its strong affinity with GSH caused the GSH-GNPs to aggregate. Then, this aggregation induced a strong fluorescence with an emission peak at 595 nm recorded by a fluorescence spectrometer. In this work, the sensitivity of the designed sensor was significantly improved by adding ethanol. The positive role of ethanol was further investigated, which demonstrated its ability to induce dense NP formation. Furthermore, the ratio of ethanol to the sample solution was optimized, which led to maximal sensitivity when detecting Pb^{2+}.

Considering that the added Pb^{2+} needed to be mixed with the testing solution and incubated for 1 min, this method required about 1 min of testing time, which showed a faster than average response time when compared to similar optical sensing platforms, with their response time ranging from 15 s to ~40 min) [32,35,42,43,45]. In this work, only the presence of Pb^{2+} caused strong luminescence of GSH-GNPs under UV light, while other ions at a 10-fold higher concentration showed no obvious responses, indicating a good selectivity for Pb^{2+} detection. The control metal ions included Ca^{2+}, Cu^{2+}, Mn^{2+}, Fe^{3+}, Fe^{2+}, and Hg^{2+}.

In another work of fluorescence-based Pb^{2+} detection, highly fluorescent silver nanoparticles (AgNPs) were synthesized and used as the probe in this competitive assay [45]. The AgNPs used in this work were initially protected by GSH from water, and the AgNP solution was orange in color due to the surface plasmon resonance band. Without GSH, AgNPs would dissolve in water and the orange fluorescence intensity would decrease. Detection of Pb^{2+} was realized when the presence of Pb^{2+} caused the dissociation of GSH from AgNPs.

To synthesize these water-soluble silver NPs, Ag^{+} was reduced to Ag^{0} using the reducing agent of hydrazine as shown in Figure 2. The aqueous solution of GSH along with NaOH was mixed into

$AgNO_3$ solution, where NaOH was used to keep the solution pH neutral. Then, hydrazine was added as a reductant and the solution was incubated for 8 hours. Orange fluorescent GSH-coated AgNPs were obtained after being washed. In the presence of Pb^{2+}, GSH would bind with Pb^{2+} to form a stable complex, leaving the AgNP surface. AgNPs would then dissolve as schematically shown in Figure 2. Here, the mechanism for complexation between Pb^{2+} and GSH was due to the cysteinyl S-donor atom in GSH. As shown in Figure 2, cysteine acts as a tridentate ligand for Pb^{2+}.

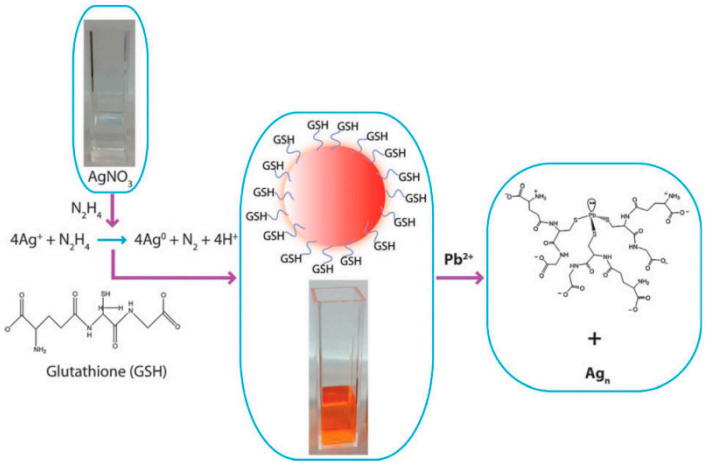

Figure 2. Fluorescence Silver Nanoparticle Synthesis Procedure and Pb^{2+} Complexation [45].

In this work, fluorescence spectra and UV-visible absorption were utilized to indicate the concentration of GSH-protected AgNPs. The initial color of the solution containing fluorescent GSH-AgNPs was orange. After adding Pb^{2+}, AgNPs were partly dissolved, resulting in a decrease in fluorescence intensity corresponding to the Pb^{2+} concentration as shown in Figure 3 [45].

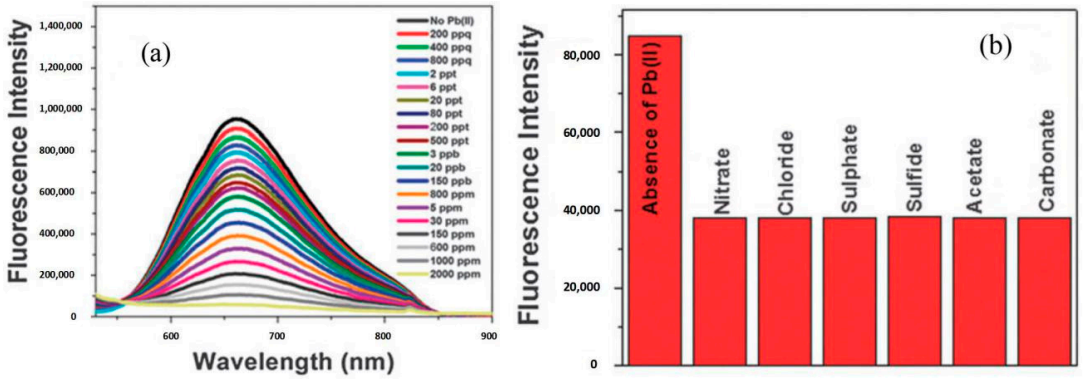

Figure 3. (**a**) Fluorescence intensity in the presence of Pb^{2+} of different concentrations. (**b**) Fluorescence intensity in the presence of different types of Pb^{2+} salts [45].

The fluorescence spectra in the presence of Pb^{2+} from 200 ppq to 2000 ppm are represented in Figure 3a, and the fluorescence intensity at 660 nm in the presence of different types of Pb^{2+} salts are given in Figure 3b. The assay took less than 20 min from Pb^{2+} binding to detection and analysis. This fluorescence assay is highly sensitive to Pb^{2+}, with a low LOD of 200 parts per quadrillion (ppq). In addition, six kinds of different lead salts, such as $PbSO_4$ and $PbCO_3$, were also tested, which exhibited similar responses as shown in Figure 3b. To demonstrate the selectivity, various alkaline or transition heavy metal ions, including Cd^{2+}, Zn^{2+}, and Hg^{2+}, were tested as shown in Figure 3b. All of the non-target metal ions were tested at a high concentration of 100 parts per billion (ppb), with no obvious decrease in the fluorescence intensity of the solutions, demonstrating good selectivity between Pb^{2+} and other HMIs. Furthermore, water samples from the Mississippi river, and dissolved plastic

toys, batteries, and paints, were tested. Those tests yielded Pb^{2+} concentrations from several tens of ppb to several hundreds of parts per million (ppm), which were in good agreement with the results by ICP-MS, demonstrating the practical value of this Pb^{2+} detection platform.

Different shapes of NPs were adopted in other reports. For example, GSH mediated end-to-end assembled gold nanorod (GNR) chains [41]. After GNRs of a certain aspect ratio and dimension were synthesized using gold seeds, they were functionalized with GSH. Because GSH tends to complex with GNRs at the endpoints of {111} facets through (-SH) groups, the appended zwitterionic of GSH at the GNR endpoints will become coupled by a two-point electrostatic interaction. The GNRs are then aligned to form a chain through the end-to-end linkage. The chain formations of the GNR were found to be broken in the presence of 0.025 mM Pb^{2+}, and a number of dimers were observed. The mechanism is depicted in Figure 4, including the processes of assembly and disassembly.

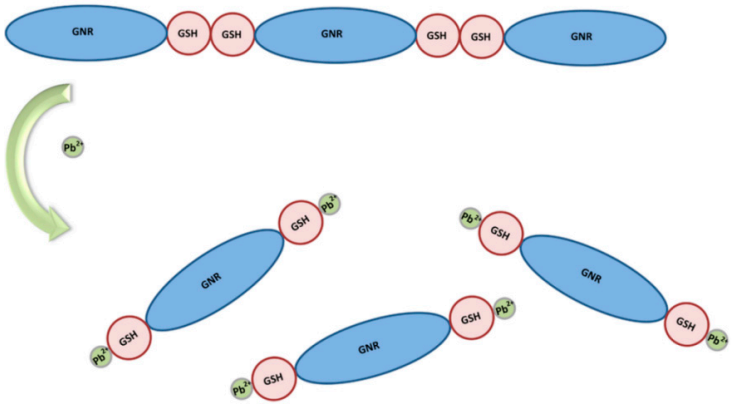

Figure 4. Assembly by GSH and disassembly by Pb^{2+} of gold nanorods (GNRs).

As discussed in Section 2, when Pb^{2+} is added, its higher affinity with the carboxyl group against other HMIs makes it possible to specifically detect Pb^{2+}. When GNR chains were disassembled due to the addition of Pb^{2+}, the size of the GNR chains decreased by more than half, i.e., about 230 nm. Dynamic light scattering (DLS) was employed for precise measurement of the hydrodynamic size of nanorods. The nanorod size measured by DLS was used to indicate the Pb^{2+} level and the selectivity of Pb^{2+} against other ions. The selectivity of this detection method was verified in the presence of various ions, such as Cu^{2+}, Hg^{2+}, Zn^{2+}, Mn^{2+}, Ni^{2+}, and NH^{4+}. The stronger affinity between Pb^{2+} and (-COOH) than that of other HMIs makes it possible to specifically detect Pb^{2+}, as discussed in Section 2. Analytes other than Pb^{2+} did not induce disintegration of the assembled chains. The LOD of this method reached 0.025 mM.

GSH-based sensing systems often operate with Pb^{2+} as their target metal ion, as discussed in the foregoing examples. Other than Pb^{2+}, arsenic (As^{3+}), nickel (Ni^{2+}), and cadmium (Cd^{2+}) detection have also been reported using GSH-capped metal NPs, which are also common HMIs of significance in environment and food safety monitoring.

A study on As^{3+} detection was conducted based on GSH/4-mercaptopyridine (4-MPY)-modified silver nanoparticles (AgNPs), and a surface-enhanced Raman scattering (SERS) spectrum was employed to find the As^{3+} concentration [46]. Both GSH and 4-MPY were conjugated to AgNPs by Ag–S or Ag–N bonds. The GSH-modified AgNPs can bind with As^{3+} through GSH by forming an As–O linkage, and 4-MPY act as the Raman reporters. One As^{3+} could link with three AgNPs to produce SERS "hot spots". Subsequently, in the absence of As^{3+}, the AgNP solution adding GSH and 4-MPY remained yellow in color. With the addition of As^{3+} into the AgNP colloidal solution, aggregation of the AgNPs occurred, and the solution's color turned to brown due to AgNP aggregation. In SERS spectra, there were some specific peaks related to As^{3+} detection, and the intensity around 1018 cm^{-1} was chosen for quantification of As^{3+}.

This sensor reached an LOD at 0.76 ppb (10.2 nM) for As^{3+} detection, and the incubation time between the addition of As^{3+} sample and the measurement was 2 min for every test. According to [46], the GSH/4-MPY-capped, AgNP-based sensor had an acceptable selectivity against other common metal ions (MIs). When testing 1.34 μM As^{3+} ions against other metal ions (Cd^{2+}, Cu^{2+}, Cr^{3+}, Zn^{2+}, Ni^{2+}, Fe^{3+}, and As^{5+} at 1.34 μM and K^{+}, Hg^{2+}, Mg^{2+}, Pb^{2+}, Ca^{2+}, and Mn^{2+} at 13.4 μM), only As^{3+} could induce a significant increase of SERS signals. Further, As^{3+} detection of drinking water was performed by the standard addition method, demonstrating recovery rates around 98.1~104.1%. While a GSH ligand could bind with many kinds of metal ions, the specificity of this assay could be attributed to the characteristics of SERS sensing, which is dependent on the charge interaction on and between AgNPs and As^{3+}, as well as the molecular structure and size.

Ni^{2+} detection by GSH-capped noble metal NPs has also been reported [47,48], which was also based on the color change between dispersed and aggregated modes of NPs. The work in [47] investigated the conditions for aggregation of GSH-GNPs induced by Ni^{2+}. For GSH-capped GNPs used in the detection of Pb^{2+}, those assays were performed in a neutral or slightly acidic environment. In [47], the assay was sensitive to Ni^{2+}, Cu^{2+}, and Zn^{2+} at pH 9.8.

The solution's pH value was carefully adjusted to observe the effects on the GSH-GNP aggregation in the presence of Ni^{2+}. UV-visible spectra were used to obtain the ratios of the absorbance intensity at 610 and 520 nm (E610/520), which indicated the degree of GNP aggregation. E610/520 changed obviously with pH, and reached a maximum when pH was about 10, which is different from the neutral pH condition for Pb^{2+} detection. Ni^{2+} had little effect on GSH-GNP aggregation when the pH value was lower than 9.0. Using FTIR, the study found that GSH was immobilized on GNPs through its cysteine sulfhydryl group and the carboxylic acid group (-COOH) of the glycine residue. Carboxyl and amine groups of the glutamyl moiety were available to bind with metal ions. At pH 6.4, after adding Ni^{2+}, only carboxyl, and not amine, groups contributed to the coordination between Ni^{2+} and GSH, while at pH 9.8, both carboxyl and amine groups participated in the coordination. The work actually found that this assay was sensitive to many other metal ions. At pH 6.4, GSH-capped GNPs exhibited weak affinity to Ni^{2+} while showing strong affinity to Cu^{2+} and Fe^{3+}, metal ions with strong affinity to the carboxyl group. At pH 9.8, GNP aggregates were formed for metal ions (Ni^{2+}, Cu^{2+}, and Zn^{2+}) with strong affinity to the deprotonated amine group. Pb^{2+} and Hg^{2+} were not tested in this work. The ratios of the absorbance intensity at 610 and 520 nm demonstrated a proportional increase with the concentration of Ni^{2+} from 10 μM to 80 μM [47].

In [48], AgNPs were used to specifically detect Ni^{2+} in water. GSH was functionalized onto the surface of AgNPs through the cysteine sulfhydryl group of GSH. It is hypothesized that carboxylate groups of the glycine moiety and amine groups from the glutamate moiety are responsible for the crosslinking between GSH-capped AgNPs and Ni^{2+}. The addition of Ni^{2+} would cause a broadening of the surface plasmon absorption band and a color change from yellow to deep orange of the solution. The ratio of the absorbance intensity (A500/A396) was used for quantification of the Ni^{2+}. The dose response showed a linear correlation with the logarithm of Ni^{2+} concentration over the range of 10^{-6}–10^{-4} mol/L with the linear detection limit of 7.5×10^{-5} mol/L. For control tests, the assay also showed a non-negligible response to Co^{2+}. Pb^{2+} was not tested. While assay conditions here are not noticeably different to those developed for Pb^{2+} detection, it should be noted that AgNPs were used here as opposed to GNPs. The generation of a plasmon resonance may have a different preference for metal ion complexation when different NPs are used.

Very recently, a competitive assay using free GSH and unmodified GNP was reported for Cd^{2+} detection [49]. Since GSH was in free form in this detection system, it could bind with metal ions or GNPs through any of the functional groups, i.e., sulfhydryl, carboxyl, and amino groups, on GSH, which may contribute to its somewhat different specificity from that of most GSH-GNP assays. The detection was based on the formation of GNP aggregates in a high-salt solution when GSH preferentially conjugated with Cd^{2+}. First, test samples were added into GSH solution, then unmodified GNPs were added. The solution was then mixed with 1 M NaCl solution and incubated

for 17 min. Without Cd^{2+}, GNPs became conjugated with GSH, and were monodispersed in the high-salt solution. When Cd^{2+} was added, GSH complexed with Cd^{2+} preferentially owing to its high affinity to Cd^{2+}. The color of aggregated GNPs showed yellow or red in dark-field images, which were observed through a dark field microscope. UV-vis absorption spectra was also used to indicate the sensitivity and selectivity of this strategy. It is necessary to point out that, in this report, the detection conditions were optimized carefully. The optimized parameters included the pH value of the solution (6.2), the salt concentration (50 mM), the GSH concentration (1.13 μM), and the reaction time (17 min). This detection method was demonstrated to be sensitive from 9.6 nM up to 11.67 μM, and it also showed a selectivity of Cd^{2+} against Pb^{2+}, Hg^{2+}, Ni^{2+}, and seven other kinds of HMIs, all at a concentration of 11.67 μM.

After surveying metallic-NP-based HMI detection platforms, we found that GSH-functionalized metallic NPs, especially GNPs, have been widely adopted for metal ion detection. Because of the stronger binding force between gold and the (-SH) group in GSH, and the specific binding ability between (-COOH) group and Pb^{2+}, Pb^{2+} is the most common HMI to be specifically detected. On the other hand, there were also some reports that detected HMIs other than Pb^{2+} under different conditions, such as high pH or using unbounded GSH. As an essential part of the HMI detection platform, a number of optical characterization methods can be used to quantify the HMI concentration, such as a UV-vis spectrophotometer, dynamic light scattering (DLS), as well as colorimetry. More HMI detection examples using NPs are listed in Section 3.3.

3.1.2. Semiconductor Quantum-Dot-Based Platforms

As an important discovery originally found in the 1990s, semiconductor quantum dots (QDs) have attracted intense research interest for their excellent luminescence properties. In contrast to traditional fluorescence techniques, QDs have advantages in excitation spectra, photo-luminescence quantum efficiency, and so on [50,51]. Reports of new QD-based sensors are on the rise. Most of the reported QD-based HMI detection schemes utilized II–VI semiconductor QDs. As an example, using Mn-doped ZnS QDs, [52] reported a Pb^{2+} detection scheme by phosphorescence measurement. Phosphorescence is generated by the energy transfer from the lowest vibrational energy layer of the excited Mn^{2+} triplet state to the vibrational energy layer of the ground state. Mn–ZnS QDs are a popular II–VI semiconductor QD for biosensor applications. Because Mn–ZnS QDs can be functionalized without using deoxidants and other inducers, they are convenient to work with. Furthermore, Mn–ZnS QDs have a long-lived doped emission, which can set the signal of Pb^{2+} detection apart from interference by autofluorescence and scattering light.

GSH was chosen to be the capping agent due to its specific binding with Pb^{2+}. To investigate the GSH coating mechanism, a Fourier transform infrared (FTIR) spectrometer was used to indicate the existence and change of functional groups or bonds. The disappearance of the S-H stretching vibrational peak was observed in the FTIR spectra after GSH was coated onto the Mn–ZnS QDs, which indicated the binding between GSH and Mn–ZnS QDs via (-SH) groups. This is similar to the immobilization mechanism when using noble metal NPs [35–37]. Furthermore, the pH was optimized to be 7.5, which was also in agreement with the Pb^{2+} detection condition discussed previously [33].

When Pb^{2+} ions were added into a solution at a pH of 7.5, the intensity quenching of GSH–Mn–ZnS QDs was observed, which was proportional to the increase in Pb^{2+} concentration. Normalized phosphorescence intensities to the blank solution (P/P_0) at 590 nm were used to quantify the Pb^{2+} concentration. The selectivity of this method was investigated by testing other common metal ions in water, including Na^{+}, Ca^{2+}, K^{+}, Mg^{2+}, Mn^{2+}, Co^{2+}, Zn^{2+}, Fe^{3+}, Cd^{2+}, Hg^{2+}, and Cu^{2+}. No metal ions yielded significant responses other than Pb^{2+}, all at a concentration of 100 nmol·L^{-1}. This demonstrated the selectivity of Pb^{2+} detection. The sensor showed a wide linear range of (1.0~100 μg/L) and an LOD of 0.45 μg/L. Furthermore, real water samples were tested containing spiked Pb^{2+}. The detection results were in good agreement with those measured by the standard ICP-MS method, indicating the practical application value of this platform.

Recently, on simultaneous HMI detection of Pb^{2+}, Cr^{3+}, and Hg^{2+} in water, a luminescence probe using layered double hydroxides (LDHs) loaded with Mn–ZnS QDs was reported [53]. In this work, the preparation of QDs on LDH was a key process. GSH–Mn–ZnS QDs nanocrystals were first synthesized. Then, a hydrothermal method was adopted to make Mg-Al-CO_3 LDHs. Lastly, GSH–Mn–ZnS QDs were immobilized on an Mg-Al-CO_3 LDH by diluting the QD solution in deionized water, adding the LDH, centrifuging the slurry, and performing a drying operation. After the solution to be tested was dropped onto the QD–LDH powder, the luminescence spectra were measured. Due to the transition of Mn^{2+} in the ZnS host lattice from the triplet state ($^4T_1$) to the ground state ($^6A_1$), Mn–ZnS QDs emit luminescence at the wavelength of 590 nm, which displays as an orange color. When any of Pb^{2+}, Cr^{3+}, and Hg^{2+} or their mixtures appear in the solution, they quench the luminescence immediately. Various solutions of metal ions were tested, including $ZnSO_4$, $AlCl_3$, $Pb(NO_3)_2$, $CrCl_3$, $HgCl_2$, $FeCl_3$, $Co(NO_3)_2$, $Cd(NO_3)_2$, phenol, and dimethylbenzene. Except for $Pb(NO_3)_2$, $CrCl_3$, and $HgCl_2$, no obvious decrease in luminescence intensity was observed for the other metal ion solutions, demonstrating the selectivity of GSH-coated QD–LDH. The focus of this research was simultaneous detection of Pb^{2+}, Cr^{2+}, and Hg^{2+}. The LOD for mixed HMIs of Pb^{2+}, Cr^{3+}, and Hg^{2+} was claimed to be 0.93 μM.

The luminescence spectra of QD–LDH in aqueous buffer with various metal ions of 1 mM are shown in Figure 5a, and the corresponding intensities are given in Figure 5b. In Figure 5, DMB (Dimethyl aminoethyl benzoate) and RhB (Rhodamine B) as well as phenol are tested as organic interferents. According to Figure 5, only Pb^{2+}, Cr^{3+}, and Hg^{2+} cause luminescence intensity quenching, while the other HMIs do not cause an obvious luminescence intensity change. In [49], the probable reason why Pb^{2+}, Cr^{3+}, and Hg^{2+} caused luminescence quenching was hypothesized as follows. It was attributed to the nonradiative recombination caused by cation exchange and competition of ligands. On the other hand, when the surface status of QDs covered with GSH were changed, the luminescence properties would be affected immediately. Even when the binding of GSH to the surfaces was only slightly broken, the luminescence intensity would be notably reduced.

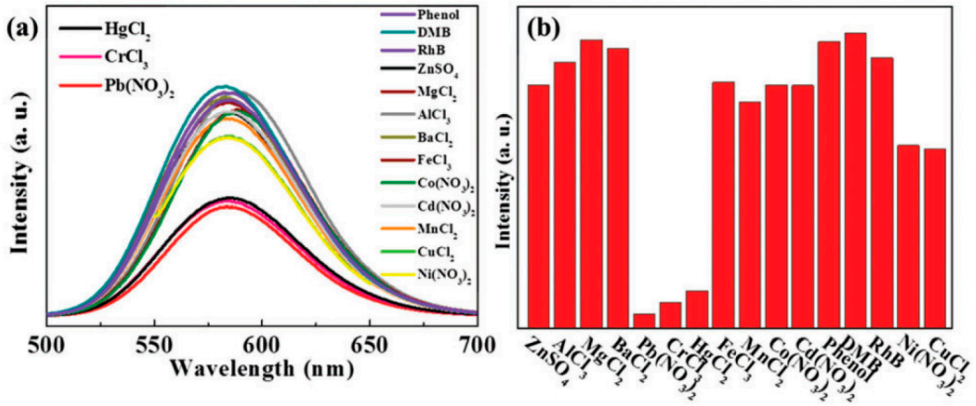

Figure 5. Detection results using a quantum dot and layered double hydroxide (QD–LDH) sensor in the presence of different metal ions: (**a**) Luminescence spectra, (**b**) intensities [53].

CdTe QDs are also extensively studied for biosensor applications. The authors in [54] reported specific detection of Pb^{2+} based on electrochemiluminescence (ECL) of CdTe QDs capped with GSH and thioglycolic acid (TGA). The general strategy and process to detect HMI was similar to the aforementioned method based on GSH-capped Mn–ZnS QDs in [53]. The primary function of GSH here was to bind Pb^{2+} with free (-COOH) groups and (-NH_2) groups. Because the ECL intensity of QDs was low when the QDs were capped with GSH alone, TGA was introduced to improve the sensitivity in this method. Both GSH and TGA were working as stabilizers for the QDs, which led to a much higher photoluminescence quantum yield. As stated in [55], a quantum yield of 63% from CdTe QDs capped by GSH and TGA was achieved as opposed to about 40% using a regular synthetic method without TGA. In [54], the ECL signal was measured in the presence of Pb^{2+}. As expected, the ECL

signal of GSH–TGA–CdTe QDs was observed to decrease. Because of the high affinity of GSH to Pb^{2+} by (-COOH) and (-NH2), the surface property of the QDs changed, leading to an obvious ECL intensity decrease. As a figure of merit, selectivity in HMI detection is always crucial. When different metal ions, such as Ca^{2+}, Na^{+}, Hg^{2+}, Cu^{2+}, Zn^{2+}, and Fe^{2+}, were added, only Hg^{2+} induced noticeable ECL quenching, showing an acceptable selectivity. The LOD of this method reached 0.26 nM, and according to the response curves, the detection time was about 15 s.

As a relatively new medium, semiconductor QDs are much more versatile and easier to use than conventional fluorescence labeling dyes due to their controllable characteristics of luminescence, which are simply dependent on crystal size. Not surprisingly, other types of QDs have also been investigated for HMI detection. Although carbon itself is not a semiconductor, carbon dots with a diameter below 10 nm exhibit typical quantum dot effects. Sulfur- and nitrogen-co-doped carbon nanoparticles (SNCNs) by GSH were reported to detect Hg^{2+} specifically [39]. A one-pot solid-phase thermal treatment of GSH was adopted to obtain the functionalized fluorescent carbon dots. Fluorescence spectra were recorded to quantify the fluorescence quenching degree related to Hg^{2+} concentration. Using the synthetic method of a one-pot solid-phase thermal treatment, there were plenty of (-SH) on the carbon dots' surface, which was presumed to provide dominant affinity to Hg^{2+} rather than other HMIs, leading to a good selectivity to other non-target ions (Ag^{+}, Al^{3+}, Ba^{2+}, Cu^{2+}, Mn^{2+}, Mg^{2+}, Na^{+}, Ni^{2+}, Pb^{2+}, Zn^{2+}, Ca^{2+}, Fe^{3+}, K^{+}, Cd^{2+}, and Fe^{2+}, 50.0 M) under the same conditions. This carbon-dot-based assay demonstrated an LOD of 0.05 nM. One test ran for about 20 min.

3.2. HMI Detection Combined with Electrochemical Techniques

Based on our survey of the field, most HMI detection techniques utilized optical techniques to extract the sensing signal. These optical methods have obvious advantages, such as visualization, but may be less advantageous when it comes to field deployability and affordable readout systems. As a result, HMI detection platforms by electrochemical techniques are also worth investigating. Among the electrochemical techniques, field effect transistors (FETs) and working electrodes are the two representative devices.

3.2.1. Field Effect Transistor-Based Platforms

An electrochemical sensing platform using a reduced graphene oxide (rGO)/gold nanoparticle (GNP) FET was developed to detect Pb^{2+} in water [34]. The rGO/GSH–GNP hybrid structure was formed on the FET channel and the GNPs were equivalent to the gate of the FET. There was an electronic transfer between the rGO and the GNPs. When the carrier concentration in the rGO changed, the external characteristics of the FET changed. Here, the rGO was used as a conducting channel to transport charge carriers. If the analytes were captured by functionalized GNPs, the charge carrier concentration would be changed, which subsequently caused a current change in the channel of FET. The current change was found to correlate with the Pb^{2+} concentration in this work, with the Pb^{2+} concentration in a range from 10 nM to 10 mM.

In this approach, amino-terminated Au electrodes as the source and drain were employed to anchor the graphene oxide. As shown in Figure 6, a monolayer α-ethyl-tryptamine (AET) film was first chemically anchored on the source and drain electrode surface. Thermal reduction of GO to rGO was performed. Then, rGO monolayer sheets were self-assembled on the AET-modified electrodes. The next step was assembling GNPs onto the rGO film. Lastly, GSH was immobilized onto GNPs on the rGO sheet surface. In this study, GSH linking with GNPs was considered through -SH linkage. In addition to the complexation mechanism introduced previously, it was hypothesized in [34] that the anions of rGO have electrostatic interactions with Pb^{2+}, improving the specific binding to Pb^{2+} by GSH. A Keithley 4200 semiconductor characterization system was used to measure the change in the FET's electrical characteristics before and after adding Pb^{2+}. The drain current (I_{ds}) acts as the indicator of Pb^{2+} concentration, which would be changed as a function of the gate voltage (V_{gs}) and the drain voltage (V_{ds}). Hence, Pb^{2+} of different concentrations could be detected.

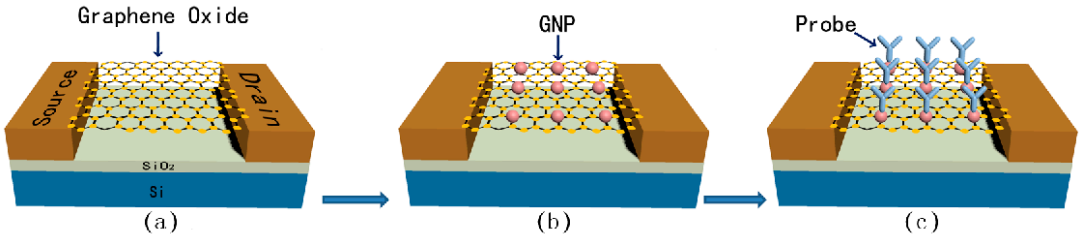

Figure 6. Fabrication of a GSH–gold nanoparticle (GNP)-decorated reduced graphene oxide (rGO) electrode sensor. (**a**) Deposition of GO monolayer sheets on the α-ethyl-tryptamine (AET)-modified electrodes, and thermal reduction of GO to rGO. (**b**) Assembly of GNPs onto the rGO film. (**c**) GSH modification of GNP-decorated rGO electrodes to form a specific receptor to Pb^{2+}.

The authors in [34] reported that the response time was as short as several seconds and the LOD of Pb^{2+} was 10 nM. Furthermore, tests of Hg^{2+}, Ag^{+}, Cd^{2+}, As^{5+}, Cu^{2+}, and Zn^{2+}, all at 10 μM, the same as the Pb^{2+} concentration, were performed as control experiments. The change of I_{ds} was very slight when the control HMIs were tested, which demonstrated the selectivity of Pb^{2+} detection.

Recently, there was another similar report on Pb^{2+} detection using an rGO-modified FET integrated with a microcontroller-based analyzer [19]. The FET consisted of an rGO channel and an Al_2O_3 thin layer working as a gate. The GNPs capped with GSH were sputtered onto the Al_2O_3 thin film gate to capture Pb^{2+} in water. Then, a microcontroller was applied to realize a capacitance measurement. The specific binding mechanism was not mentioned in this report. However, based on the foregoing discussion in this review, the mechanism of specific detection of Pb^{2+} using GSH-GNPs is attributed to the strong affinity between Pb^{2+} and (-COOH) as described in Section 2. Interestingly, the drain current was not adopted to indicate the analyte concentration as is commonly done. Instead, a square pulse wave in series with a reference resistor was used to calculate the time constant of the distorted signal across the drain–source interface, apparently extracting the gate capacitance change due to Pb^{2+} binding.

For specificity, this sensor exhibited a specific response to Pb^{2+} against other common HMIs as well as cations in water, such as Zn^{2+}, Mg^{2+}, Fe^{3+}, and $HAsO_4^{2-}$. Here, the Pb^{2+} concentration was 2.5 ppb and the others were of a concentration of 10 ppb. The response for Pb^{2+} was at least 12 times larger than those of the control subjects, demonstrating a good selectivity for Pb^{2+} detection. A rapid response of 1~2 s and an overall assay time of ~10 s were achieved, which was fast compared with other existing HMI detection techniques. The LOD of this platform was below 1 ppb, and the approximate linear operational range was 5~20 ppb, which was around the limit amount (15 ppb) of lead that the U.S. EPA imposes as a restriction for drinking water. As an added bonus, this work produced a compact platform utilizing a preprogrammed microcontroller.

3.2.2. Working-Electrode-Based Platforms

Over the years, nanostructures have become a must to obtain good sensitivity. The electrodes used in this method are all modified with nanomaterials on their surface. Based on a graphene-modified electrode, an electrochemical detection of Cd^{2+} was performed by square wave anodic stripping voltammetry (SWASV) [56]. A thoroughly cleaned glassy-carbon electrode (GCE) was adopted to be the working device. Then, an rGO/carboxymethyl cellulose (CMC)/glutathione (GSH) film was coated on the polished bare electrode by coating their suspension followed by drying steps. By analyzing the electrochemical behavior, the rGO/CMC/GSH nanocomposite exhibited a good performance of carrier transport. Electrochemical impedance spectroscopy (EIS) was used to characterize the functionalized electrode. The rGO/CMC/GSH/GCE showed a smaller semicircle in the Nyquist plot compared with other electrodes, which indicated low interface resistance and rapid interfacial charge transfer, which can be considered as advantages when using this nanocomposite structure.

The functionalized GCE is described in the schematic diagram of Figure 7. Detection of Cd^{2+} (2 nM) using bare and modified electrodes was compared under the voltage of (−1.0~−0.6 V). The

response peak current of rGO/CMC/GSH/GCE was much sharper and higher than those of control electrodes, such as GO/GCE, rGO/GCE, and rGO/CMC/GCE. Three reasons were attributed to the enhanced peak current. There were a larger surface area and better conductivity of the electrode from GO; more (-OH) and (-COOH) groups provided by CMC, which can chelate with Cd^{2+}; and eight heterogeneous active sites in GSH for Cd^{2+} coordination.

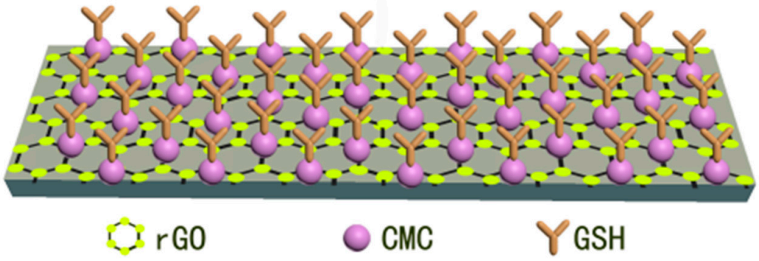

Figure 7. Schematic diagram of rGO/carboxymethyl cellulose (CMC)/GSH/-functionalized glassy-carbon electrode (GCE).

To demonstrate the selectivity of Cd^{2+}, equimolar samples at 10 nM of Cu^{2+}, Zn^{2+}, Hg^{2+}, and Cd^{2+} were tested. Except for Cd^{2+} and Pb^{2+}, the other HMIs showed no obvious response. As for Pb^{2+}, the authors claimed that its current peak was lower than that of Cd^{2+}. So, there existed specificity for Cd^{2+} in this detection method. According to this research, the LOD of Cd^{2+} reached 0.05 nM, and the detection time was optimized to be 120 s considering the Cd^{2+} deposition process onto the electrode.

In another variation of nanomaterial-modified electrodes, a screen-printed carbon nanofiber electrode combined with GSH was developed for metal ions detection using a voltammetric measurement [57]. In this report, the GSH-modified electrode was electrografted onto a screen-printed carbon nanofiber substrate (GSH-SPCNFE). In contrast to the classical screen-printed carbon electrode modified with GSH (GSH-SPCE), this method exhibited much better electrochemical characterization, indicating better GSH immobilization. An electrochemical workstation was used for stripping measurements, and the sensing was performed based on a three-electrode system in acetate buffer (pH 4.5). Ag/AgCl/KCl and Pt wire worked as the reference and auxiliary electrode, respectively, and a GSH-SPCNFE was used as the working electrode. Voltammetry was applied to analyze the target metal ion complexation level after the metal ions had been deposited onto the electrode for 120 s. As for the binding mechanism, the authors believed that the thiol group in the GSH played an important role to complex with HMI in their experiment. Pb^{2+} and Cd^{2+} could be detected at two different potentials, both with an LOD of about 3.0 μg/L.

In addition, a practical sample of a wastewater-certified reference material (ERM®-CA713) was tested. In this application, Pb^{2+} was specifically detected as expected. Because the selected reference material contained Cr, Cu, Mn, Ni, and so on, which were at concentrations not lower than Pb^{2+}, and the detected concentration of Pb^{2+} was in agreement with the certified metal value, the selectivity of this HMI detection technique was verified. Although the LOD was not so outstanding, these modified electrodes could be stored for weeks without obvious activity decline, showing a good potential towards commercialization.

In principle, the ready-made or commercial electronic devices, such as GCE and FET, are advantageous in transferring the HMI concentration information to an electrical signal. Although electrochemical detection of HMIs is not as popular as optical detection, electrochemical sensing platforms also have merits, in that they are more convenient, compact, and cheaper to implement.

3.3. Summary of HMI Detection Platforms Using GSH

In summary, GSH has been adopted as the probe molecule in a variety of HMI detection platforms. These detection platforms have demonstrated good detection performance, such as a low LOD and a fast response. Some of them have been applied to practical samples with acceptable outcomes.

The platforms discussed above present commonly reported detection methods, and are not an exhaustive list of all existing GSH-based HMI sensors. Table 1 gives a more comprehensive summary of recently reported HMI detection platforms using GSH. In addition to the examples discussed in the review, Table 1 includes some less-used detection methods with their operational characteristics. As every application has its own unique requirements, different considerations go into choosing a certain detection platform. For example, it is difficult to find a sensor with high sensitivity and a very fast response at the same time. Some trade-off is needed when choosing a detection method. It is our hope that this summary will provide some guidance for choosing a suitable strategy to detect certain HMIs.

Table 1. Recent Achievements in Heavy Metal Ion (HMI) Detection Platforms Using GSH.

Signal Transduction	Sensor Structure	HMI Target	Detection Limit	Linear Range	Response Time	References
Optical methods						
Colorimetry	Gold NPs	Pb	0.1 μM	0.1~50 μM	20 ~ 25 min	[43]
	Silver NPs	Pb	1 nM	Not mentioned	At least 10 min	[32]
	Gold NPs	Cd	4.3 pM	17 pM~16.67 nM	About 17 min	[49]
Localized surface plasmon resonance	Gold NPs	Pb	50 pM	0.1 nM~10 μM	15 min	[33]
Fluorescence	Gold NPs	Pb	0.1 μM	2~350 μM	About 1 min	[44]
	Silver NPs	Pb	0.6 pM (200 ppq)	60 pM~2.4 nM (20~800 ppt estimated)	Less than 20 min	[45]
Surface-enhanced Raman scattering	Silver NPs	As^{3+}	10.2 nM (0.76 ppb)	53.7 nM~4.0 μM (4~300 ppb)	At least 2 min	[46]
Whispering gallery mode	Gold NPs	Pb	0.05 nM	2.40~48.26 nM	About 40 min	[35]
Spectrophotometry	Mn-doped ZnS QDs	Pb	2.2 nM (0.45 μg/L)	4.9 nM~0.49 μM (1.0~100 μg/L)	Not mentioned	[52]
	Mn-doped ZnS QDs	Pb, Cr, Hg	0.93 μM for mixed HMIs	1 μM~1 mM	Not mentioned	[53]
	CdTe QDs	Pb	0.26 nM	0.8~15 nM	About 15 s	[54]
	Carbon QDs	Hg	0.05 nM	1 nM~50 μM	At least 20 min	[39]
	Silver NPs	Ni^{2+}	75 μM	About 75 μM~1 mM	Not mentioned	[48]
	Gold Nanostars	Pb	0.5 μM	About 0.5~4 μM	About 30 min	[42]
Dynamic Light Scattering	Gold Nanorod Chains	Pb	0.025 mM	Not mentioned	Not mentioned	[41]
Electrochemical methods						
Square Wave Anodic Stripping Voltammetry, SWASV	Magnetic NPs	Cd, Pb	1.6 nM (0.182 μg/L); 0.8 nM (0.172 μg/L)	4.4~879 nM (0.5~100 μg/L), 2.3~460 nM (0.5~100 μg/L)	210 s 210 s	[40]
	Glassy-Carbon Electrode	Cd	0.05 nM	2~20 nM	120 s	[56]
	Carbon Paste Electrode	Cd	8.5 nM (2 ppb)	4.2~420 nM (1~100 ppb)	Longer than 7 min	[58]
Differtial pulsed anodic striping voltammetry, DPASV	Screen-Printed Carbon Nanofiber Electrode	Pb, Cd	~0.1 nM (~3 μg/L)	About 0.3~4.5 nM (about 10~150 μg/L)	120 s	[57]
FET (Drain current)	Field effect Transistor	Pb	10 nM	10 nM~10 μM	1–2 s	[34]
FET (Pulse-driven capacitance)	Gate Capacitance	Pb	<4.8 nM (<1 ppb)	24~96 nM (5~20 ppb)	1–2 s	[19]

4. Concluding Remarks

Heavy metal contamination is one of the major concerns in an ever-increasingly industrialized world. Broad applications of heavy metals in modern industries, agriculture, and medicines have led to their widespread distribution in the environment. The toxic effects of heavy metals have proven to be the source of many health risks. Some of them, such as lead and mercury, are considered to be highly hazardous to humans even at a trace level, and are ranked as priority metals that are of public health significance. Therefore, it is crucial to develop effective detection techniques that are user-friendly, affordable, fast, and sensitive for point-of-need detection and monitoring.

Among various approaches to detect HMIs, GSH is gradually becoming a popular probe due to its strong affinity with several HMIs and its flexibility with the sensing methods and materials. With multiple functional groups of (-SH), (-COOH), and (-NH2) on it, GSH is a versatile probe capable of binding with several metal ions, either individually or together at the same time. By adjusting the testing conditions, such as the solution's pH value, GSH exhibited a tunable complexation ability to different HMIs, with maximum affinity for Pb^{2+} at a pH of around 7. While most GSH-based HMI detection platforms were designed to specifically detect Pb^{2+}, targets other than Pb^{2+} have also been reported using GSH probes under different conditions.

When using GSH as a probe, the benefit is more than rich functional groups on its surface for HMI detection. A variety of sensing strategies can be realized, owing to GSH's compatibility with diverse sensor materials and signal transduction methods. This comprehensive review emphasizes the advances made in the development of novel optical, electrochemical, and other GSH-based sensors for the detection of toxic heavy metal ions. Based on their signal transduction strategies, the reported HMI sensors can be broadly classified into optical methods and electrical methods. Optical detection is typically used in coordination with noble metal NPs and semiconductor QDs, while electrochemical methods often use FETs and working electrodes as the transducers. Each has its strengths and weaknesses. The optical methods use a new batch of NPs or QDs for each test, avoiding any need to modify the detectors themselves, while electrochemical methods require a newly modified device for each test. Based on the review, electrochemical methods are quicker to obtain results than optical methods with comparable LODs, and optical methods are less susceptible to interferences than electrochemical methods.

To make these systems suitable for real-world applications, such as environmental monitoring and biological testing, much effort is needed to overcome the challenges that these sensors currently face, such as assay robustness, qualitative and quantitative analysis, control of sample temperature and pH, user-friendliness, and cost-effectiveness. Further, for field-deployable applications, miniaturization of these sensors and detectors, and simplicity and automation in the measurement procedure, are additional challenges.

Author Contributions: Conceptualization, J.Z. and J.W.; Methodology, J.W. and J.Z.; Software, X.S.; Validation, J.W.; Formal Analysis, X.S.; Investigation, J.Z.; Resources, J.W. and J.Z.; Data Curation, X.S.; Writing-Original Draft Preparation, X.S.; Writing-Review & Editing, J.Z. and J.W.; Visualization, J.Z.; Supervision, J.W.; Project Administration, J.W.; Funding Acquisition, J.W. and J.Z.

Funding: This research was funded by the University of Tennessee Initiative for PON/POC Nanobiosensing, Institute for a Secure and Sustainable Environment, the US NSF CPS/USDA NIFA (Grant no. 2017-67007-26150), the open research fund of the Key Laboratory of MEMS of the Ministry of Education, Southeast University, China, and the National Natural Science Foundation of China (Grant no. 51728502).

Conflicts of Interest: The authors declare no conflict of interest.

References

1. Bansod, B.K.; Kumar, T.; Thakur, R.; Rana, S.; Singh, I. A review on various electrochemical techniques for heavy metal ions detection with different sensing platforms. *Biosens. Bioelectron.* **2017**, *94*, 443–455. [CrossRef] [PubMed]

2. Cui, L.; Wu, J.; Ju, H. Electrochemical sensing of heavy metal ions with inorganic, organic and bio-materials. *Biosens. Bioelectron.* **2015**, *63*, 276–286. [CrossRef] [PubMed]
3. Pujol, L.; Evrard, D.; Serrano, K.G.; Freyssinier, M.; Cizsak, A.R.; Gros, P. Electrochemical sensors and devices for electrochemical assay in water: The French groups' contribution. *Front. Chem.* **2014**, *2*, 19. [CrossRef]
4. Gumpu, M.B.; Sethuraman, S.; Krishnan, U.M.; Rayappan, J.B.B. A review on detection of heavy metal ions in water—An electrochemical approach. *Sens. Actuators B Chem.* **2015**, *213*, 515–533. [CrossRef]
5. Vázquez-González, M.; Carrillo-Carrion, C. Analytical strategies based on quantum dots for heavy metal ions detection. *J. Biomed. Opt.* **2014**, *19*, 1–12. [CrossRef] [PubMed]
6. Ginya, M.A.; Idris, M.B.; Zakariyya, U.A.; Singh, D.; Yakasai, H.; Sani, N. The role of some antioxidants on absorption, desorption and elimination of lead and iron: An in-vivo study. *Eur. J. Biomed. Pharm. Sci.* **2016**, *3*, 528–531.
7. Afkhami, A.; Soltanifelehgari, F.; Madrakian, T.; Ghaedi, H.; Rezaeivala, M. Fabrication and application of a new modified electrochemical sensor using nano-silica and a newly synthesized schiff base for simultaneous determination of Cd^{2+}, Cu^{2+} and Hg^{2+} ions in water and some foodstuff samples. *Anal. Chim. Acta* **2013**, *771*, 21–30. [CrossRef] [PubMed]
8. Sharma, B.; Singh, S.; Siddiqi, N.J. Biomedical implications of heavy metals induced imbalances in redox systems. *BioMed. Res. Int.* **2014**, *2014*, 640754. [CrossRef]
9. Gong, T.; Liu, J.; Liu, X.; Liu, J.; Xiang, J.; Wu, Y. A sensitive and selective platform based on CdTe QDs in the presence of L-cysteine for detection of silver, mercury and copper ions in water and various drinks. *Food Chem.* **2016**, *213*, 306–312. [CrossRef] [PubMed]
10. Turdean, G.L. Design and development of biosensors for the detection of heavy metal toxicity. *Int. J. Electrochem.* **2011**, *2011*, 343125. [CrossRef]
11. Gao, C.; Yu, X.Y.; Xiong, S.Q.; Liu, J.H.; Huang, X.J. Electrochemical detection of arsenic(III) completely free from noble metal: Fe_3O_4 microspheres-roomtemperature ionic liquid composite showing better performance than gold. *Anal. Chem.* **2013**, *85*, 2673–2680. [CrossRef] [PubMed]
12. Array, G.; Merkoci, A. Nanomaterials application in electrochemical detection of heavy metals. *Electrochim. Acta* **2012**, *84*, 49–61. [CrossRef]
13. Sitko, R.; Janik, P.; Zawisza, B.; Talik, E.; Margui, E.; Queralt, I. Green approach for ultra trace determination of divalent metal ions and arsenic species using totalreflection X-ray fluorescence spectrometry and mercapto-modified graphene oxide nanosheets as a novel adsorbent. *Anal. Chem.* **2015**, *87*, 3535–3542. [CrossRef] [PubMed]
14. Liu, X.; Zhu, Z.; Li, H.; He, D.; Li, Y.; Zheng, H.; Gan, Y.; Li, Y.; Belshaw, N.S.; Hu, S. Liquid spray dielectric barrier discharge induced plasma-chemical vapor generation for the determination of lead by ICPMS. *Anal. Chem.* **2017**, *89*, 6827–6833. [CrossRef] [PubMed]
15. Feng, W.; Xue, X.; Liu, X. One-step, room-temperature, colorimetric detection of mercury (Hg^{2+}) using DNA/nanoparticle conjugates. *J. Am. Chem. Soc.* **2008**, *130*, 3244–3245.
16. Li, S.; Xu, L.; Ma, W.; Kuang, H.; Wang, L.; Xu, C. Triple raman label-encoded gold nanoparticle trimers for simultaneous heavy metal ion detection. *Small* **2015**, *11*, 3435–3439. [CrossRef]
17. Skotadis, E.; Tsekenis, G.; Chatzipetrou, M.; Patsiouras, L.; Madianos, L.; Bousoulas, P.; Zergioti, I.; Tsoukalas, D. Heavy metal ion detection using dnazyme-modified platinum nanoparticle networks. *Sens. Actuators B Chem.* **2017**, *239*, 962–969. [CrossRef]
18. Kullick, T.; Quack, R.; Röhrkasten, C.; Pekeler, T.; Scheper, T.; Schügerl, H.C.K. Pbs-field-effect-transistor for heavy metal concentration monitoring. *Chem. Eng. Technol.* **2010**, *18*, 225–228. [CrossRef]
19. Maity, A.; Sui, X.; Tarman, C.R.; Pu, H.; Chang, J.; Zhou, G.; Ren, R.; Mao, S.; Chen, J. Pulse-driven capacitive lead ion detection with reduced graphene oxide field-effect transistor integrated with an analyzing device for rapid water quality monitoring. *ACS Sens.* **2017**, *2*, 1653–1661. [CrossRef]
20. Hang, R.; Kang, Y.; Gladwin, E.; Claus, R.O. Selective detection of heavy metal ions by self assembled chemical field effect transistors. *Appl. Phys. Lett.* **2015**, *106*, 402647.
21. March, G.; Nguyen, T.D.; Piro, B. Modified electrodes used for electrochemical detection of metal ions in environmental analysis. *Biosensors* **2015**, *5*, 241–275. [CrossRef]
22. Blake, D.A.; Jones, R.M.; Ii, R.C.B.; Pavlov, A.R.; Darwish, I.A.; Yu, H. Antibody-based sensors for heavy metal ions. *Biosens. Bioelectron.* **2001**, *16*, 799–809. [CrossRef]

23. Saidur, M.R.; Aziz, A.R.; Basirun, W.J. Recent advances in dna-based electrochemical biosensors for heavy metal ion detection: A review. *Biosens. Bioelectron.* **2017**, *90*, 125–139. [CrossRef] [PubMed]
24. Zhan, S.; Wu, Y.; Wang, L.; Zhan, X.; Zhou, P. A mini-review on functional nucleic acids-based heavy metal ion detection. *Biosens. Bioelectron.* **2016**, *86*, 353–368. [CrossRef] [PubMed]
25. Ritchie, S.M.C.; Kissick, K.E.; Bachas, L.G.; Sikdar, S.K.; Parikh, C.; Bhattacharyya, D. Polycysteine and other polyamino acid functionalized microfiltration membranes for heavy metal capture. *Environ. Sci. Technol.* **2001**, *35*, 3252–3258. [CrossRef] [PubMed]
26. Neupane, L.N.; Oh, E.T.; Park, H.J.; Lee, K.H. Selectively and sensitively detection of heavy metal ions in 100% aqueous solution and cells with a fluorescence chemosensor based on peptide using aggregation induced emission. *Anal. Chem.* **2016**, *88*, 3333–3340. [CrossRef] [PubMed]
27. Farzin, L.; Shamsipur, M.; Sheibani, S. A review: Aptamer-based analytical strategies using the nanomaterials for environmental and human monitoring of toxic heavy metals. *Talanta* **2017**, *174*, 619–627. [CrossRef]
28. Oroval, M.; Coll, C.; Bernardos, A.; Marcos, M.D.; Martínez-Máñez, R.; Shchukin, D.G.; Sancenón, F. Selective fluorogenic sensing of As(III) using aptamer-capped nanomaterials. *ACS Appl. Mater. Interfaces* **2017**, *9*, 11332–11336. [CrossRef]
29. Zhou, S.F.; Wang, J.J.; Gan, L.; Han, X.J.; Fan, H.L.; Mei, L.Y.; Huang, J.; Liu, Y.Q. Individual and simultaneous electrochemical detection toward heavy metal ions based on l-cysteine modified mesoporous $MnFe_2O_4$ nanocrystal clusters. *J. Alloys Compd.* **2017**, *721*, 492–500. [CrossRef]
30. Zhang, L.; Xu, C.; Li, B. Simple and sensitive detection method for chromium(VI) in water using glutathione-capped CdTe quantum dots as fluorescent probes. *Microchim. Acta* **2009**, *166*, 61–68. [CrossRef]
31. Mah, V.; Jalilehvand, F. Lead(II) complex formation with glutathione. *Inorg. Chem.* **2012**, *51*, 6285–6298. [CrossRef] [PubMed]
32. Anambiga, I.V.; Suganthan, V.; Arunai Nambi Raj, N.; Buvaneswari, G.; Sampath Kumar, T.S. Colorimetric Detection of lead ions using glutathione stabilized silver nanoparticles. *Int. J. Sci. Eng. Res.* **2013**, *4*, 710–715.
33. Feng, B.; Zhu, R.; Xu, S.; Chen, Y.; Di, J. A sensitive LSPR sensor based on glutathione-functionalized gold nanoparticles on a substrate for the detection of Pb^{2+} ions. *RSC Adv.* **2018**, *8*, 4049–4056. [CrossRef]
34. Zhou, G.; Chang, J.; Cui, S.; Pu, H.; Wen, Z.; Chen, J. Real-time, selective detection of Pb^{2+} in water using a reduced graphene oxide/gold nanoparticle field-effect transistor device. *ACS Appl. Mater. Inter.* **2014**, *6*, 19235–19241. [CrossRef] [PubMed]
35. Panich, S.; Wilson, K.A.; Nuttall, P.; Wood, C.K.; Albrecht, T.; Edel, J.B. Label-free Pb(II) whispering gallery mode sensing using self-assembled glutathione-modified gold nanoparticles on an optical microcavity. *Anal. Chem.* **2014**, *86*, 6299–6306. [CrossRef] [PubMed]
36. Beqa, L.; Singh, A.K.; Khan, S.A.; Senapati, D.; Arumugam, S.R.; Ray, P.C. Gold nanoparticle-based simple colorimetric and ultrasensitive dynamic light scattering assay for the selective detection of Pb(II) from paints, plastics, and water Samples. *ACS Appl. Mater. Interfaces* **2011**, *3*, 668–673. [CrossRef] [PubMed]
37. Kim, I.B.; Dunkhorst, A.; Gilbert, J.; Bunz, U.H.F. Sensing of lead ions by a carboxylate-substituted PPE: Multivalency effects. *Macromolecules* **2005**, *38*, 4560–4562. [CrossRef]
38. Vila-Viçosa, D.; Teixeira, V.H.; Santos, H.A.F.; Machuqueiro, M. Conformational Study of GSH and GSSG Using Constant-pH Molecular Dynamics Simulations. *J. Phys. Chem. B* **2013**, *117*, 7507–7517. [CrossRef]
39. Wang, W.; Lu, Y.C.; Huang, H.; Wang, A.J.; Chen, J.R.; Feng, J.J. Solvent-free synthesis of sulfur- and nitrogen-co-doped fluorescent carbon nanoparticles from glutathione for highly selective and sensitive detection of mercury(II) ions. *Sens. Actuators B Chem.* **2014**, *202*, 741–747. [CrossRef]
40. Baghayeri, M.; Amiri, A.; Maleki, B.; Alizadeh, Z.; Reiser, O. A simple approach for simultaneous detection of cadmium(II) and lead(II) based on glutathione coated magnetic nanoparticles as a highly selective electrochemical probe. *Sens. Actuators B Chem.* **2018**, *273*, 1442–1450. [CrossRef]
41. Durgadas, C.V.; Lakshmi, V.N.; Sharma, C.P.; Sreenivasan, K. Sensing of lead ions using glutathione mediated end to end assembled gold nanorod chains. *Sens. Actuators B Chem.* **2011**, *156*, 791–797. [CrossRef]
42. D'Agostino, A.; Taglietti, A.; Bassi, B.; Donà, A.; Pallavicini, P. A naked eye aggregation assay for Pb^{2+} detection based on glutathione-coated gold nanostars. *J. Nanopart. Res.* **2014**, *16*, 2683. [CrossRef]
43. Chai, F.; Wang, C.; Wang, T.; Li, L.; Su, Z. Colorimetric detection of Pb^{2+} using glutathione functionalized gold nanoparticles. *ACS Appl. Mater. Interfaces* **2010**, *2*, 1466–1470. [CrossRef]

44. Zhang, H.; Wang, S.; Chen, Z.; Ge, P.; Jia, R.; Xiao, E.; Zeng, W. A turn-on fluorescent nanoprobe for lead(II) based on the aggregation of weakly associated gold(I)-glutathione nanoparticles. *Microchim. Acta* **2017**, *184*, 4209–4215. [CrossRef]
45. Singh, A.K.; Kanchanapally, R.; Fan, Z.; Senapati, D.; Ray, P.C. Synthesis of highly fluorescent water-soluble silver nanoparticles for selective detection of Pb(II) at the parts per quadrillion (PPQ) level. *Chem. Commun.* **2012**, *48*, 9047–9049. [CrossRef]
46. Li, J.; Chen, L.; Lou, T.; Wang, Y. Highly sensitive SERS detection of As^{3+} ions in aqueous media using glutathione functionalized silver nanoparticles. *ACS Appl. Mater. Interfaces* **2011**, *3*, 3936–3941. [CrossRef]
47. Fu, R.; Li, J.; Yang, W. Aggregation of glutathione-functionalized Au nanoparticles induced by Ni^{2+} ions. *J. Nanopart. Res.* **2012**, *14*, 929. [CrossRef]
48. Li, H.; Cui, Z.; Han, C. Glutathione-stabilized silver nanoparticles as colorimetric sensor for Ni. *Sens. Actuators B Chem.* **2009**, *143*, 87–92. [CrossRef]
49. Li, L.; Liu, B.; Chen, Z. Colorimetric and dark-field microscopic determination of cadmium(II) using unmodified gold nanoparticles and based on the formation of glutathione-cadmium(II) complexes. *Microchim. Acta* **2019**, *186*, 37. [CrossRef]
50. Nightingale, A.M.; deMelloa, J.C. Improving the ensemble optical properties of InP quantum dots by indium precursor modification. *J. Mater. Chem. C* **2016**, *4*, 8454–8458. [CrossRef]
51. Choi, D.B.; Kim, S.; Yoon, H.C.; Ko, M.; Yang, H.; Do, Y.R. Color-tunable Ag-In-Zn-S quantum-dot light-emitting devices realizing green, yellow and amber emissions. *J. Mater. Chem. C* **2017**, *5*, 953–959. [CrossRef]
52. Chen, J.; Zhu, Y.; Zhang, Y. Glutathione-capped Mn-doped ZnS quantum dots as a room-temperature phosphorescence sensor for the detection of pb^{2+} ions. *Spectrochim. Acta A* **2016**, *164*, 98–102. [CrossRef]
53. Liu, J.; Lv, G.; Gu, W.; Li, Z.; Tang, A.; Mei, L. A novel luminescence probe based on layered double hydroxides loaded with quantum dots for simultaneous detection of heavy metal ions in water. *J. Mater. Chem. C* **2017**, *5*, 5024–5030. [CrossRef]
54. Wang, H.; Chen, Q.; Tan, Z.; Yin, X.; Lun, W. Electrochemiluminescence of CdTe quantum dots capped with glutathione and thioglycolic acid and its sensing of Pb^{2+}. *Electrochim. Acta* **2012**, *72*, 28–31. [CrossRef]
55. Tian, J.; Liu, R.; Zhao, Y.; Xu, Q.; Zhao, S. Controllable synthesis and cell-imaging studies on CdTe quantum dots together capped by glutathione and thioglycolic acid. *J. Colloid Interfaces Sci.* **2009**, *336*, 504–509. [CrossRef]
56. Priya, T.; Dhanalakshmi, N.; Thennarasu, S.; Thinakaran, N. Ultra sensitive detection of Cd (II) using reduced graphene oxide/carboxymethyl cellulose/glutathione modified electrode. *Carbohyd. Polym.* **2018**, *197*, 366–374.
57. Pérez-Ràfols, C.; Serrano, N.; Díaz-Cruz, J.M.; Ariño, C.; Esteban, M. Glutathione modified screen-printed carbon nanofiber electrode for the voltammetric determination of metal ions in natural samples. *Talanta* **2016**, *155*, 8–13. [CrossRef]
58. Kaabi, R.; Abderrabba, M.; Gómez-Ruiz, S.; Hierro, I.D. Bioinspired materials based on glutathione-functionalized SBA-15 for electrochemical Cd(II) detection. *Microporous Mesoporous Mater.* **2016**, *234*, 336–346. [CrossRef]